Available online at www.sciencedirect.com
ScienceDirect
Nuclear Physics B Proceedings Supplement 00 (2014) 1–6
Nuclear Physics B Proceedings Supplement

Searches for invisible decay modes of the Higgs boson with the CMS detector

Daniele Trocino, on behalf of the CMS Collaboration

Northeastern University, 360 Huntington Ave, Boston, MA 02115, US

Abstract

A search for Higgs boson invisible decay modes has been carried out in events where the Higgs boson is produced in association with a Z boson as well as through vector boson fusion. In the associated production search, electron, muon and b-quark pair decay modes of the Z boson are considered. The analyses are based on pp collision data collected with the CMS detector at the LHC collider at centre-of-mass energies of 7 and 8 TeV, corresponding to integrated luminosities of 5 fb^{-1} and 20 fb^{-1}, respectively. No evidence of a signal has been found and upper limits on the invisible branching fraction are obtained and interpreted in a Higgs portal model of dark matter interactions.

Keywords: LHC, CMS, Higgs, Dark Matter

1. Introduction

Since the observation of a new boson with mass of about 125 GeV at the Large Hadron Collider (LHC) [1, 2], all measurements of its properties have indicated compatibility with the standard model (SM) Higgs boson. However, the associated uncertainties are large, and the possibility for non-SM properties remains.

Decays of the Higgs boson to undetectable particles are possible in a wide range of models. In general, interactions of the Higgs boson with the unknown dark matter (DM) sector may introduce invisible decay modes. In so-called "Higgs-portal" models of DM [3, 4], the Higgs boson serves as mediator between the SM particles and the DM particle.

Indirect constraints on non-SM decay modes of the Higgs boson have been inferred from the visible SM decay modes [5]. The resulting upper limit on the non-SM branching fraction is 0.32, at 95% confidence level (CL). Direct searches for invisible Higgs boson decays, H(inv), are possible by requiring that the Higgs boson recoils against a visible system.

Here we report searches for H(inv) with the Compact Muon Solenoid (CMS) detector [6] in two production modes: the vector boson fusion (VBF), where the Higgs boson is produced in association with two quarks, and the ZH mode, where the Z boson decays to leptons ($\text{Z}(\ell\ell)\text{H(inv)}$ channel) or a $\text{b}\bar{\text{b}}$ quark pair ($\text{Z}(\text{b}\bar{\text{b}})\text{H(inv)}$ channel). All the searches are conducted using the 8 TeV data sample collected by the CMS Collaboration during 2012, corresponding to an integrated luminosity of about 19.5 fb^{-1}. The search in the $\text{Z}(\ell\ell)\text{H(inv)}$ channel also uses the 7 TeV dataset collected during 2011, corresponding to 4.9 fb^{-1}.

2. Search in vector boson fusion

In the VBF mode, the Higgs boson is produced in association with two jets separated by a large rapidity gap and having high invariant mass. The rapidity gap between the two jets is characterized by reduced hadronic activity. Events are thus collected with a trigger that requires missing transverse energy ($E_{\text{T}}^{\text{miss}}$), in association with a pair of jets with high transverse momentum (p_{T}), large pseudorapidity (η) separation, $\Delta\eta_{j_1,j_2} = \left|\eta_{j_1} - \eta_{j_2}\right|$, and high invariant mass, M_{j_1,j_2}. A tightened version of the same selection is applied offline, namely $E_{\text{T}}^{\text{miss}} > 130\,\text{GeV}$, $p_{\text{T}}^{j_{1,2}} > 50\,\text{GeV}$, $\left|\eta_{j_{1,2}}\right| < 4.7$, $\eta_{j_1}\cdot\eta_{j_2} < 0$, $\Delta\eta_{j_1,j_2} > 4.2$, and $M_{j_1,j_2} > 1100\,\text{GeV}$. Back-

Email address: daniele.trocino@cern.ch (Daniele Trocino)

grounds Z($\ell\ell$)+jets and W($\ell\nu$)+jets are rejected by vetoing any event with an identified electron or muon with $p_{\mathrm{T}} > 10\,\mathrm{GeV}$. Multijet backgrounds are suppressed by requiring the azimuthal separation between the tag jets to be small, $\Delta\phi_{j_1,j_2} < 1.0\,\mathrm{rad}$. Finally, a veto is applied to any event that has an additional jet with $p_{\mathrm{T}} > 30\,\mathrm{GeV}$ and η between those of the two tag jets. After these requirements, a hypothetical invisible Higgs boson with mass of 125 GeV produced via VBF is reconstructed with an efficiency of $6.8 \cdot 10^{-3}$. Assuming the SM production cross section and an invisible branching fraction $\mathcal{B}(\mathrm{H} \to \mathrm{inv}) = 100\%$, this corresponds to a yield of 210 events.

The dominant background, Z($\nu\nu$)+jets, is estimated from data using observable Z($\mu\mu$) decays. A Z control region is defined by requiring an oppositely-charged pair of well-identified muons with invariant mass between 60 and 120 GeV. The number of Z($\nu\nu$) events in the signal region is then predicted scaling the number of Z($\mu^+\mu^-$) events in the control region by the ratio of the different cross sections and efficiencies of the two processes, obtained from simulation. In a similar way, the W($\ell\nu$)+jets background ($\ell = \mathrm{e}, \mu, \tau$) is estimated from single-lepton events. The control samples are defined requiring an isolated electron or muon, or a hadronically-decaying τ, and vetoing any additional leptons. The extrapolation from each control region to the signal region is performed using factors evaluated from simulation. The multijet background in the signal region is estimated using events that pass the same requirements as the signal, but fail the central-jet veto. The number of events in the control region is then multiplied by the ratio of events passing and failing the central-jet veto. This factor is measured in a sample with $E_{\mathrm{T}}^{\mathrm{miss}} < 130\,\mathrm{GeV}$. The remaining SM backgrounds in the signal region—$\mathrm{t\bar{t}}$, single-top, VV and Z/γ^*($\ell\ell$)+jets processes—are estimated from simulation. The total expected background is 332±36 (stat)± 45 (syst).

The dominant systematic uncertainty in the signal yield is due to jet and $E_{\mathrm{T}}^{\mathrm{miss}}$ energy scale and resolution. Theoretical uncertainties in the VBF signal cross section, resulting from PDF modeling and factorization and renormalization scale uncertainties, are also considered. The signal simulation includes a small contribution from the gluon-fusion process, where the jets are produced through initial-state radiation (ISR). The large uncertainty in the ISR modeling has a modest overall effect. Other small uncertainties arise from the integrated luminosity and lepton identification efficiencies. The total uncertainty in the signal yield is estimated to be 14%. The uncertainty in the background yield is dominated by the large statistical uncertainties in the V+jets background estimates, due to the control samples in data, and by the systematic uncertainty in the control-to-signal region translation factors for the V+jets backgrounds. Large uncertainties are assigned to the multijet background, but they have a small impact on the overall background uncertainty. For the minor backgrounds estimated from MC, additional uncertainties arise from the cross sections, which are set according to the corresponding CMS cross section measurements. The total uncertainty in the background yield is 18%.

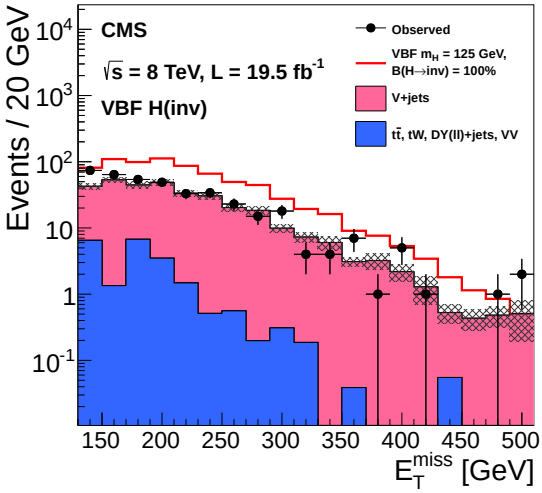

Figure 1: The $E_{\mathrm{T}}^{\mathrm{miss}}$ distribution in data and MC after the full selection in the VBF search signal region. The background is normalized to the estimates obtained from data, and shown cumulatively, with the total systematic uncertainty shown as a hatched region. Note that the QCD multijet background is not shown due to limited MC statistics, which results in a small apparent discrepancy between data and the backgrounds at low $E_{\mathrm{T}}^{\mathrm{miss}}$ values. The cumulative effect of a signal from a Higgs boson with SM VBF production cross section, $m_{\mathrm{H}} = 125\,\mathrm{GeV}$, and $\mathcal{B}(\mathrm{H} \to \mathrm{inv}) = 100\%$ is also shown.

Figure 1 shows the $E_{\mathrm{T}}^{\mathrm{miss}}$ distribution in data and simulated backgrounds in the signal region. The 390 observed events are compatible with the background prediction. In absence of deviations from the SM expectation, 95% CL upper limits are set on the Higgs boson VBF production cross section times invisible branching fraction.

3. Search in the Z($\ell\ell$)H(inv) channel

The final state in the Z($\ell\ell$)H(inv) channel consists of a pair of high-p_{T} isolated leptons from the Z boson decay, high $E_{\mathrm{T}}^{\mathrm{miss}}$ from the undetectable Higgs boson decay products, and limited jet activity. Events are thus collected using dielectron and dimuon triggers, together with single-muon triggers that allow recovery of

some residual trigger inefficiencies. The offline selection starts by requiring two well-identified, isolated leptons of the same flavor and opposite sign (e^+e^- or $\mu^+\mu^-$), each with $p_T > 20$ GeV. The invariant mass of the pair must be within 15 GeV of the Z boson mass. To reduce the large background from the Drell–Yan (DY) process $Z^{(*)}/\gamma^*(\ell\ell)$+jets, where the E_T^{miss} arises from mismeasurement, any event containing two or more jets with $p_T > 30$ GeV is rejected. The remaining zero- and one-jet samples are treated separately in the analysis because of their significantly different signal-to-background ratios. To reduce the $W(\ell\nu)Z(\ell\ell)$ background, events containing additional identified electrons or muons with $p_T > 10$ GeV are rejected. The top-quark background is further suppressed by rejecting events containing an identified b-jet with $p_T > 20$ GeV or a soft muon. The remaining event selection uses three variables to suppress reducible backgrounds like DY and top-quark production: $E_T^{miss} > 120$ GeV, $\left|\Delta\phi\left(\ell\ell, E_T^{miss}\right)\right| > 2.7$, and $\left|E_T^{miss} - p_T^{\ell\ell}\right|/p_T^{\ell\ell} < 0.25$, where $p_T^{\ell\ell}$ is the transverse momentum of the dilepton system. The efficiency of the full selection for the $Z(\ell\ell)H(inv)$ signal at $m_H = 125$ GeV is 5.6%.

After the full selection, the dominant backgrounds arise from WZ and ZZ processes, which are modeled using MC simulation and normalized to next-to-leading order (NLO) cross sections [7]. The DY background is modeled using a large-statistics control sample of events with a single isolated photon produced in association with jets (γ + jets). Photon production resembles the DY process in all important aspects: production mechanism, underlying event conditions, pileup scenario, and hadronic recoil. The kinematic distributions and overall normalization of the photon events are matched to $Z(\ell\ell)$ in data through p_T^γ-dependent event weights. The remaining background processes, $t\bar{t}$, single-top, and WW, do not involve Z boson production, and are referred to as "non-resonant backgrounds". These backgrounds are estimated using a control sample in data, consisting of events with opposite-charge different-flavor dilepton pairs ($e^\pm\mu^\mp$) that otherwise pass the full selection. The backgrounds in the e^+e^- and $\mu^+\mu^-$ final states are then estimated by applying scale factors (α_{ee}, $\alpha_{\mu\mu}$) to the number of events in the control sample. Factor α_{ee} ($\alpha_{\mu\mu}$) is measured as the ratio of the number of ee ($\mu\mu$) events to the number of e μ events in the sidebands of the Z peak ($40 < M_{\ell\ell} < 70$ GeV and $110 < M_{\ell\ell} < 200$ GeV). In order to reduce the statistical uncertainties in α_{ee} and $\alpha_{\mu\mu}$, the selection of ee, $\mu\mu$, and e μ events in the sidebands is looser than in the signal region.

The most important uncertainties in this search are those associated with theory, resulting from PDF modeling and factorization and renormalization scales, which affect both the signal acceptance and the dominant W Z and Z Z backgrounds. An additional uncertainty in the ZH production cross section stems from next-to-next-to-leading order (NNLO) QCD corrections [8] and NLO electroweak corrections [9, 10, 11]. NLO electroweak corrections to the ZZ and WZ background processes [12] are also included. The uncertainties related to jet and E_T^{miss} energy scale and resolution, lepton p_T scale, and reconstruction efficiency affect the signal and all backgrounds. Uncertainties of approximately 100%, derived by comparing different estimation methods in data and conducting closure tests in simulation, are assigned to the non-resonant backgrounds. However, their contribution to the total background uncertainty is small. The signal efficiency uncertainty is estimated to be about 12%, and the total uncertainty in the background estimations is about 15%.

The total number of observed events in the 7 TeV and 8 TeV samples is 134, with an estimated background of about 138 events and expected signal yield of 35 events for $m_H = 125$ GeV and $\mathcal{B}(H \to inv) = 100\%$. The final limits on a signal are determined using a profile-likelihood fit to selected distributions in the signal region. For the 7 TeV data, the transverse mass of the dilepton-E_T^{miss} system is used, defined as

$$m_T = \sqrt{2p_T^{\ell\ell}E_T^{miss}\left[1 - \cos\Delta\phi\left(\ell\ell, E_T^{miss}\right)\right]}.$$

For the 8 TeV data, the limits are computed using the two-dimensional distribution of the azimuthal dilepton separation, $\Delta\phi_{\ell,\ell}$, and m_T. In the fit, the shapes and normalizations of the signal and of each background are allowed to vary within their uncertainties, and correlations in the sources of systematic uncertainty are taken into account. Figure 2 shows the m_T distribution in the 8 TeV data. It can be seen that the observed data are consistent with the predicted backgrounds.

4. Search in the Z(bb̄)H(inv) channel

The $Z(b\bar{b})H(inv)$ search is characterized by final states with large E_T^{miss} and a pair of b-jets consistent with a $Z \to b\bar{b}$ decay. A suite of different triggers is used throughout the data taking to adapt to the increasing LHC instantaneous luminosity. Each trigger requires the presence of E_T^{miss}, with thresholds ranging from 80 to 100 GeV, and two jets with $|\eta| < 2.5$ and p_T thresholds varying from 20 to 60 GeV. Additional requirements are imposed on the two jets, e.g. a minimum

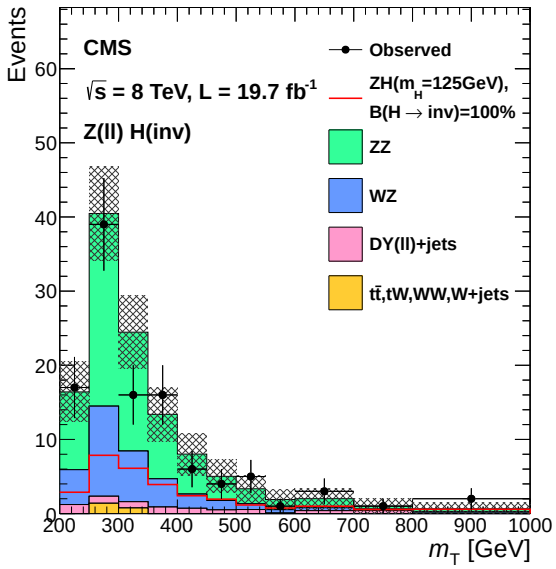

Figure 2: Dilepton-$E_{\mathrm{T}}^{\mathrm{miss}}$ transverse mass distribution at 8 TeV in data and simulation. The expected background distributions are displayed cumulatively, while a signal corresponding to $m_{\mathrm{H}} = 125\,\mathrm{GeV}$ and $\mathcal{B}(\mathrm{H} \to \mathrm{inv})$ =100% is superimposed separately. The total statistical and systematic uncertainty in the background is shown as a hatched region.

threshold on the vectorial sum of the two jets p_{T}, or being identified by the combined secondary vertex (CSV) b-tagging algorithm, which combines information from track impact parameters and secondary vertices to identify b-jets and reject jets originating from light quarks, c quarks or gluons. The offline selection starts by requiring large $E_{\mathrm{T}}^{\mathrm{miss}}$, which is used to define three separate regions with different sensitivities, and thus treated separately in the limit setting: low-, intemediate-, and high-$E_{\mathrm{T}}^{\mathrm{miss}}$ regions, with $E_{\mathrm{T}}^{\mathrm{miss}}$ values in the ranges of 100-130 GeV, 130-170 GeV, and $>$ 170 GeV, respectively. The Z boson candidate is reconstructed from a pair of jets with $|\eta| < 2.5$ and $p_{\mathrm{T}} > 60$ and 30 GeV, with further requirements on the p_{T} and invariant mass of the dijet system. The two jets are also required to be tagged by the CSV discriminator. To reduce the $\mathrm{t\bar{t}}$ and WZ backgrounds, events with isolated leptons with $p_{\mathrm{T}} > 15\,\mathrm{GeV}$ are rejected. The multijet background is reduced to negligible levels by imposing several requirements which ensure that the $E_{\mathrm{T}}^{\mathrm{miss}}$ does not originate from mismeasured jets, e.g. the minimum azimuthal separation between the $E_{\mathrm{T}}^{\mathrm{miss}}$ direction and the closest jet, and a minimum threshold on the $E_{\mathrm{T}}^{\mathrm{miss}}$ significance, defined as the ratio of the $E_{\mathrm{T}}^{\mathrm{miss}}$ and the square root of the scalar sum of transverse energy of all particle candidates. After the full selection, the efficiency for a signal with $m_{\mathrm{H}} = 125\,\mathrm{GeV}$ and $\mathcal{B}(\mathrm{H} \to \mathrm{inv}) = 100\%$ is 4.8%. The final signal yield is estimated using a boosted decision tree (BDT), by fitting the BDT output for background and signal to that obtained from data.

All backgrounds are modeled using simulation. For the main backgrounds, i.e. Z+jets, W+jets, and $\mathrm{t\bar{t}}$, the normalizations are obtained from control regions in data. For the Z and W backgrounds, different control regions are defined depending on the number of b-jets in the event, 0, 1 or 2. The normalization of each background is obtained with simultaneous fits to the CSV distributions in each control region.

The main uncertainties in the signal yield arise from factorization and renormalization scales, PDF modeling, QCD NNLO and electroweak NLO corrections. The dominant uncertainty in the background yield is due to the normalization procedure for Z+jets, W+jets, and $\mathrm{t\bar{t}}$ processes. Other uncertainties affect both the normalization and BDT output shape of signal and backgrounds, such as jet and $E_{\mathrm{T}}^{\mathrm{miss}}$ energy scales and resolutions, trigger efficiency, and b-tagging efficiency. The total uncertainties in the signal and background yields are 11% and 12%, respectively.

Figure 3 shows an example of BDT output for the high-$E_{\mathrm{T}}^{\mathrm{miss}}$ region. The data are compatible with the background estimations. Limits are determined using a fit to the BDT output distributions, separately for each Higgs boson mass hypothesis.

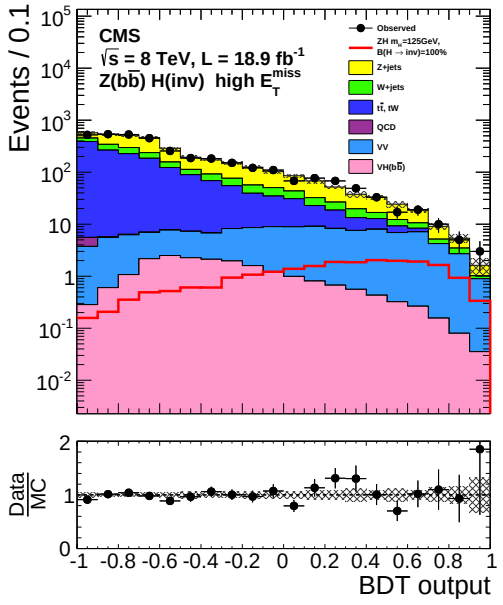

Figure 3: Distributions of the Z(bb̄)H(inv) BDT output in the high-$E_{\mathrm{T}}^{\mathrm{miss}}$ bin after the full selection criteria. The simulated background contributions are displayed cumulatively, while a signal corresponding to $m_{\mathrm{H}} = 125\,\mathrm{GeV}$ and $\mathcal{B}(\mathrm{H} \to \mathrm{inv})$ =100% is superimposed. The uncertainty in the background is shown as a hatched region.

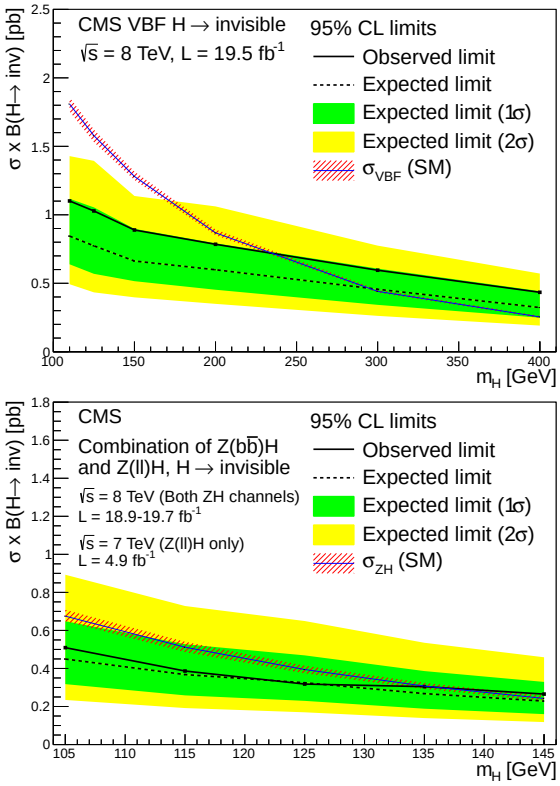

Figure 4: Expected and observed 95% CL upper limits on the production cross section times invisible branching fraction in the VBF channel (top) and in the ZH channel (bottom).

5. Cross section limits

Limits are calculated using a CL_S method [13, 14], where systematic uncertainties are incorporated as nuisance parameters. Limits are also set on the production cross section times invisible branching fraction normalized to the SM production cross section, $\xi = \sigma \cdot \mathcal{B}(\mathrm{H} \to \mathrm{inv})/\sigma_{\mathrm{SM}}$. Figure 4 shows the observed and median expected 95% CL limits on the Higgs boson production cross section times invisible branching fraction, as a function of the Higgs boson mass, for VBF production (top) and for the ZH production, combining the searches in the $\ell\ell + E_{\mathrm{T}}^{\mathrm{miss}}$ and $\mathrm{b\bar{b}} + E_{\mathrm{T}}^{\mathrm{miss}}$ channels (bottom). The observed (expected) limits on ξ for a Higgs boson of mass 125 GeV set by the three individual searches are 0.65 (0.49), 0.83 (0.86), and 1.82 (1.99) in the VBF, $\mathrm{Z}(\ell\ell)\mathrm{H}(\mathrm{inv})$, and $\mathrm{Z}(\mathrm{b\bar{b}})\mathrm{H}(\mathrm{inv})$ channels, respectively. By assuming production cross sections as for the SM Higgs boson, these individual results may be combined and interpreted as a limit on the invisible branching fraction of the 125 GeV Higgs boson. The statistical combination fully accounts for correlations between nuisance parameters in the individual searches, such as the uncertainties on jet energy scale and signal cross sections. The resulting 95% CL limit on ξ is shown in Fig. 5. For $m_{\mathrm{H}} = 125$ GeV, the observed (expected) upper limit on the invisible branching fraction is 0.58 (0.44) at 95% CL, and 0.51 (0.38) at 90% CL.

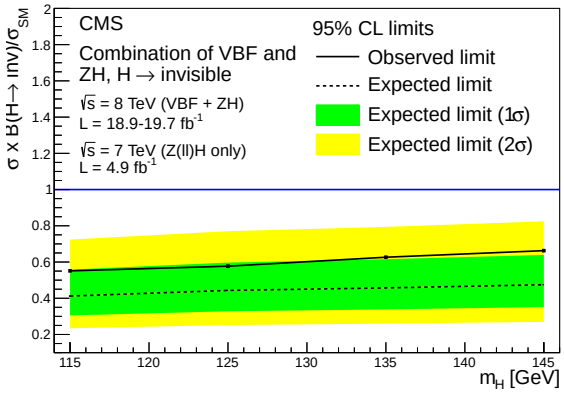

Figure 5: Expected and observed 95% CL upper limits on $\xi = \sigma \cdot \mathcal{B}(\mathrm{H} \to \mathrm{inv})/\sigma(\mathrm{SM})$.

6. Dark matter interactions

The experimental upper limit on $\mathcal{B}(\mathrm{H} \to \mathrm{inv})$ can be interpreted in the context of a Higgs-portal model of DM interactions. In these models, a hidden sector can provide stable DM particles with direct renormalizable couplings to the SM Higgs sector. In direct detection experiments, the elastic interaction between DM and nuclei exchanged through the Higgs boson results in nuclear recoil which can be reinterpreted in terms of DM mass, M_χ, and DM-nucleon cross section. If the DM candidate has a mass below $m_{\mathrm{H}}/2$, the invisible Higgs boson decay width, Γ_{inv}, can be translated to a spin-independent DM-nucleon elastic cross section for scalar, vector, and fermionic DM candidates. Figure 6 shows upper limits at 90% CL on the DM-nucleon cross section as a function of the DM mass, derived from the experimental upper limit on $\mathcal{B}(\mathrm{H} \to \mathrm{inv})$ for $m_{\mathrm{H}} = 125$ GeV, in the scenarios where the DM candidate is a scalar, a vector, or a Majorana fermion.

7. Conclusions

A search for invisible decays of Higgs bosons has been performed, using the vector boson fusion and associated ZH production modes, with $\mathrm{Z} \to \ell\ell$ or $\mathrm{Z} \to \mathrm{b\bar{b}}$. No evidence for a signal is observed, and limits are placed in terms of $\sigma \cdot \mathcal{B}(\mathrm{H} \to \mathrm{inv})$ and $\sigma \cdot \mathcal{B}(\mathrm{H} \to \mathrm{inv})/\sigma_{\mathrm{SM}}$. By assuming standard model production

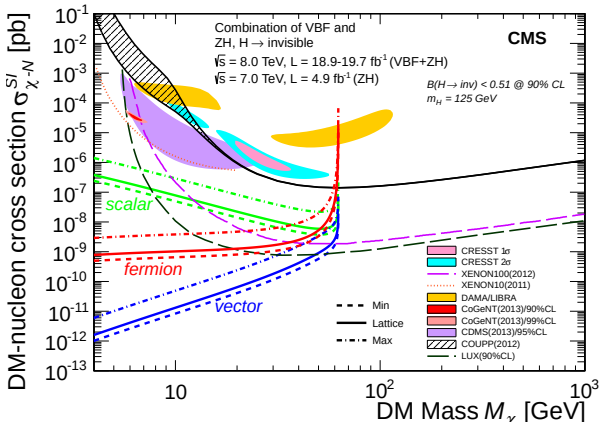

Figure 6: Upper limits on the spin-independent DM-nucleon cross section $\sigma^{\mathrm{SI}}_{\chi-\mathrm{N}}$ in Higgs-portal models, derived for $m_{\mathrm{H}} = 125\,\mathrm{GeV}$ and $\mathcal{B}(\mathrm{H} \to \mathrm{inv}) < 0.51$ at 90% CL, as a function of the DM mass. Limits are shown separately for scalar, vector and fermion DM. The solid lines represent the central value of the Higgs-nucleon coupling, while the dashed and dot-dashed lines represent lower and upper bounds on this parameter. Other experimental results are shown for comparison, from the CRESST [15], XENON10 [16], XENON100 [17], DAMA/LIBRA [18], CoGeNT [19], CDMS II [20], COUPP [21], LUX [22] Collaborations.

cross sections, the upper limit on the invisible branching fraction of a Higgs boson with $m_{\mathrm{H}} = 125\,\mathrm{GeV}$ is found to be 0.58, with an expected limit of 0.44, at 95% confidence level. Finally, the result is interpreted in a Higgs-portal model of dark matter. Strong limits are obtained on the dark matter-nucleon cross section for light dark matter.

References

[1] G. Aad, et al., Observation of a new particle in the search for the standard model Higgs boson with the ATLAS detector at the LHC, Phys. Lett. B 716 1.

[2] S. Chatrchyan, et al., Observation of a new boson at a mass of 125 GeV with the CMS experiment at the LHC, Phys. Lett. B 716 30.

[3] B. Patt, F. Wilczek, Higgs-field portal into hidden sectors (2006). arXiv:hep-ph/0605188.

[4] A. Djouadi, O. Lebedev, Y. Mambrini, J. Quevillon, Implications of LHC searches for Higgs–portal dark matter, Phys. Lett. B 709 65.

[5] Precise determination of the mass of the Higgs boson and studies of the compatibility of its couplings with the standard model, Tech. Rep. CMS-PAS-HIG-14-009, CERN, Geneva (2014).

[6] S. Chatrchyan, et al., The CMS experiment at the CERN LHC, JINST 3 (2008) S08004.

[7] J. M. Campbell, R. K. Ellis, MCFM for the Tevatron and the LHC, Nucl. Phys. Proc. Suppl. 205 (2010) 10.

[8] G. Ferrera, M. Grazzini, F. Tramontano, Associated WH production at hadron colliders: a fully exclusive QCD calculation at NNLO, Phys. Rev. Lett. 107 152003.

[9] M. Ciccolini, A. Denner, S. Dittmaier, Strong and electroweak corrections to the production of Higgs + 2jets via weak interactions at the LHC, Phys. Rev. Lett. 99 161803.

[10] M. Ciccolini, A. Denner, S. Dittmaier, Electroweak and QCD corrections to Higgs production via vector-boson fusion at the LHC, Phys. Rev. D 77 013002.

[11] A. Denner, S. Dittmaier, S. Kallweit, A. Muck, Electroweak corrections to Higgs-strahlung off W/Z bosons at the Tevatron and the LHC with HAWK, JHEP 1203 075.

[12] A. Bierweiler, T. Kasprzik, J. H. Kühn, Vector-boson pair production at the LHC to $O(\alpha^3)$ accuracy, JHEP 12 71.

[13] A. L. Read, Presentation of search results: the cl_s technique, J. Phys. G 28 (2002) 2693.

[14] T. Junk, Confidence level computation for combining searches with small statistics, Nucl. Instrum. Meth. A 434 (1999) 435.

[15] G. Angloher, et al., Results from 730 kg days of the CRESST-II Dark Matter search, Eur. Phys. J. C 72 (2012) 1971. arXiv:1109.0702.

[16] X. Collaboration, Search for light dark matter in xenon10 data, Phys. Rev. Lett. 107 (2011) 051301.

[17] X. Collaboration, Dark Matter Results from 225 Live Days of XENON100 Data, Phys. Rev. Lett. 109 181301.

[18] C. Savage, G. Gelmini, P. Gondolo, K. Freese, Compatibility of DAMA/LIBRA dark matter detection with other searches, JCAP 04 (2009) 010. arXiv:0808.3607.

[19] C. Collaboration, CoGeNT: A search for low-mass dark matter using p-type point contact germanium detectors, Phys. Rev. D 88 (2013) 012002. arXiv:1208.5737.

[20] C. Collaboration, Silicon Detector Dark Matter Results from the Final Exposure of CDMS II, Phys. Rev. Lett. 111 (2013) 251301. arXiv:1304.4279.

[21] C. Collaboration, First dark matter search results from a 4-kg CF_3I bubble chamber operated in a deep underground site, Phys. Rev. D 86 (2012) 052001. arXiv:1204.3094.

[22] L. Collaboration, First results from the LUX dark matter experiment at the Sanford Underground Research Facility, Phys. Rev. Lett. 112 (2014) 091303. arXiv:1310.8214.